文章编号：1001 -9014(2019)05-0566-06

DOI:10. 11972/j. issn. 1001-9014. 2019. 05. 004

Numerical study of a tungsten twin-cross-grating-based solar selective absorber

ZHANG Jing-Ru[1], TU Hua-Tian[1], ZANG Kai-Yan[1], HU Er-Tao[2], ZHANG Rong-Jun[1], ZHENG Yu-Xiang[1], WANG Song-You[1], ZHAO Hai-Bin[1], YANG Yue-Mei[1], CHEN Liang-Yao[1*]

(1. Department of Optical Science and Engineering, Fudan University, Shanghai, 200433, China;
2. College of Electronic and Optical Engineering & College of Microelectronics, Nanjing University of Posts and Telecommunications, Nanjing 210023, China)

Abstract: Based on the six-layered metal/dielectric film structure, a new 2D tungsten twin-cross-grating-based solar selective absorber (SSA) has been proposed to improve the optical absorption in the solar radiation region. The weighted average absorptivity before the cut-off wavelength is about 96. 5%, and the calculated emissivity at 850 K is about 0. 086. The mechanisms of high absorption in the solar region have been further analyzed by field intensity distribution in the SSA structure. The absorber also has the feature to be less polarization-dependent and broad angular-independent up to 50°, which satisfies the required conditions of the SSA device in applications.

Key words: solar selective absorber, photonic crystal absorbers, high absorption, low emittance

PACS: 78. 20. Bh, 78. 20. nb

基于W双十字形微结构的太阳能选择性吸收薄膜的数值研究

张静如[1], 涂华恬[1], 臧恺岩[1], 胡二涛[2], 张荣君[1], 郑玉祥[1], 王松有[1], 赵海斌[1], 杨月梅[1], 陈良尧[1*]

(1. 复旦大学 光科系与工程系, 上海 200433;
2. 南京邮电大学 电子与光学工程学院&微电子学院, 江苏 南京 210023)

摘要: 提出一种基于金属-介质六层膜的高太阳辐射吸收的新型双十字形微结构, 计算显示其加权平均吸收率在截止波长前的光谱区约为96.5%, 850 K温度的辐射率为0.086. 通过场图分析对太阳能波段的光热吸收机制进行了探讨. 不同入射角情况下的计算结果显示, 基于双十字形微结构的太阳能选择性吸收薄膜可具有低偏振依赖性, 以及小于50°入射角条件下的低入射角依赖性特点, 将能够满足太阳能选择性吸收器件的应用需求.

关 键 词: 太阳能选择性吸收薄膜; 光子晶体吸收器; 高吸收; 低辐射

中图分类号: O43 **文献标识码**: A

Introduction

Solar thermal conversion, one of the common methods of solar energy application, has been widely used in solar thermal systems, like the solar thermoelectric generators (STEGs) and solar thermophotovoltaics (STPVs). Solar selective absorbers (SSAs) are the crucial parts playing the significant role in the solar thermal systems. According to previous research, SSAs could be divided into six types: intrinsic absorbers, semiconductor-metal tandems, multilayer absorbers, cermet absorbers, structure absorbers and photonic crystal absorbers [1]. The high solar-to-thermal conversion of SSAs should perform with the optical reflectance spec-

Received date: 2019-03-08, **revised date**: 2019-07-14 **收稿日期**: 2019-03-08, **修回日期**: 2019-07-14

Foundation items: Supported by National Natural Science Foundation of China (61427815)

Biography: ZHANG Jing-Ru (1994-), female, Shanghai, master. Research area involves optic science and engineering, E-mail: 16210720015@fudan. edu. cn

[*] **Corresponding author**: E-mail: lychen@fudan. ac. cn

trum of an ideal reflector in thermal radiation regions. In addition, other features like the thermal stability, polarization insensitivity and incident angle insensitivity are also important in broad applications. Metamaterial absorbers have been wildly used in the terahertz and infrared frequency regions[2-3], and also show great potential to be used as SSAs for their large optical bandgaps and outstanding control over the photonic density of states. For working in the higher temperature conditions, the most commonly applied materials in study to absorb the solar energy in high efficiency are transition metals which have the advantages of high melting point and low vapor pressure for solar energy absorption. The relatively poor incidence-angle-dependent properties of one-dimensional (1D) metallic photonic crystals (PhC) of SSAs have seriously limited the applications in solar thermal systems. Thus, attention has been paid to the two-dimensional (2D) metallic photonic crystals studies more often in solar thermal applications. Recently different materials like W, Ta, W-Ta alloys and Ti have been proposed to design the SSAs in the solar thermal systems, especially in STPV systems[4-8].

As one kind of transitional metals, tungsten with the melting point up to 3410°C shows excellent performance in the PhC-based SSAs. The cylinder-shaped 2D-PhC-based SSA was designed with measured absorptivity higher than 0.9 in average in the 0.5-to-1.75 μm wavelength region with predicted emissivity lower than 0.13[9]. The cuboid-shaped 2D-PhC-based SSA was numerically simulated with total solar absorptivity higher than 88% at the normal incidence condition and the emissivity lower than 0.03 at 100°C[10]. The structures with 2D symmetric patterns as mentioned above were numerically proved to show strong wavelength selectivity. Some of them also show superior properties in both of incidence angle and polarization independence. However, accompanied by high absorption of the SSA structures, there are some low absorption valleys occurred in the solar region. It indicates that the absorptivity valley of the cuboid-shaped 2D PhC-based SSA even reaches to a value lower than 0.8 at the wavelength of about 600 nm.

In this work, we numerically design a new SSA absorber consisting of a twin-cross tungsten structure to be put on a six-layered film structure. Although multilayered SSAs seem to show high absorption property in the solar region, it is hard for the absorption spectrum to get a peak value higher than 0.98. With the 2D grating structure being put on the multilayered film, the absorption of the SSA absorber would potentially have the peak value close to 1. The absorption properties of these metamaterial SSAs were studied in the 250 nm to 25 μm spectral region by means of the finite-difference time-domain (FDTD) method. The incidence-angle-dependent polarization effects were also discussed in detail.

1 Basic ideas of simulation

The absorptivity at the solar spectrum and emissivity at IR region are two crucial parameters for high-efficiency SSAs with certain operating temperature T. The absorptivity α is calculated by the following equation:

$$\alpha = \frac{\int_0^\infty A(\lambda) L_{sun} \mathrm{d}\lambda}{\int_0^\infty L_{sun} \mathrm{d}\lambda}, \quad , \quad (1)$$

where $A(\lambda)$ is the absorptivity as a function of wavelength, and L_{sun} is the AM1.5 solar radiation. In addition, the emissivity ε is given over the full hemisphere:

$$\varepsilon = \frac{\int_0^{2\pi}\int_0^{\pi/2}\int_0^\infty E(T,\lambda)\varepsilon(\theta,\lambda)\sin(\theta)\cos(\theta)\mathrm{d}\lambda\mathrm{d}\theta\mathrm{d}\varphi}{\pi\int_0^\infty E(T,\lambda)\mathrm{d}\lambda}, \quad (2)$$

where $\varepsilon(\theta, \lambda)$ is emissivity depending on the wavelength and heat-emission angle in the space, and $E(T,\lambda)$ represents Plank's blackbody radiation, given in the following equation:

$$E(T,\lambda) = \frac{2hc^2}{\lambda^5}\left[\exp\left(\frac{hc}{\lambda k_B T}\right) - 1\right]^{-1} \quad . \quad (3)$$

An ideal selective absorber ($\alpha = 1$, $\varepsilon = 0$), as seen the spectra with dashed lines shown in Fig. 1(a), is discussed first. While the solar energy is radiated to earth in the 250-to-2 500 nm wavelength region, the high absorptivity in the region does not certainly lead to a high efficiency, since the solar-to-thermal conversion efficiency will also be affected by the value of emissivity. The blackbody emissivity in the wavelength region of 2-2.5 μm will not be negligible. Thus, the concept in the SSA design to have a cut-off wavelength λ_c is significant, implying that in the wavelength region over the point of λ_c, the thermal loss due to heat radiation will become a dominant factor to affect the solar-to-thermal conversion efficiency. Because of the red-shift of blackbody radiation with increasing temperature, λ_c would decrease with increasing temperature. λ_c is also determined by optical concentration C, shown in Fig. 1(b), which is corresponding to reports in the previously published literatures [11]. The curves of optimal cut-off wavelength are cliff-fractured in some points, because the solar radiation reaching at the earth surface will approach to zero in the wavelength region from 1.4-to-1.8 μm due to strong atmospheric absorption [12]. In fact, even the absorptivity of the real absorber can reach to the value close to 1, the emissivity will inevitably not be zero. When the absorptivity is higher than 95%, the optimal cut-off wavelength is almost unchanged with absorptivity in the situation without optical concentration. However, the spectrum of the optimal cut-off wavelength is sensitive to the emissivity, are shown in Fig. 1(c).

A unit cell of the designed metamaterial SSA structure consisting of 2D periodic tungsten gratings being put on a six-layered film structure is depicted in Fig. 2. The 2D periodic tungsten gratings have a grating period of Λ, two x-y-crosses with spans of x and y, width w, and thickness h. In addition, the six-layered film structure is set as SiO_2(60 nm)/W(6 nm)/SiO_2(65 nm)/W(12 nm)/SiO_2(50 nm)/W(100 nm) from top to bottom. The incident wave vector represents the electromagnetic wave with the incident angle θ and polarization angle ψ. ψ =

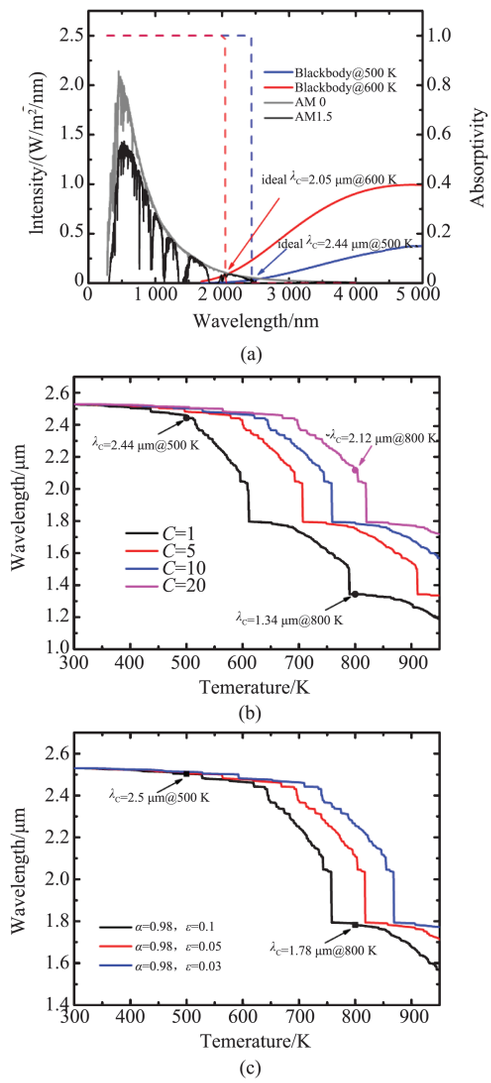

Fig. 1 (a) Solar radiation reaching at the earth surface (AM 1.5) and blackbody radiation of an absorber at 500 K and 600 K. The ideal absorption spectra of absorbers at 500 K and 600 K are shown in blue and red dashed lines with different values of cut-off wavelength λ_c, respectively. (b) In ideal conditions, the curves of cut-off wavelength and temperature in different optical concentrations. (c) The spectra of cut-off wavelength changing with temperature under the condition of different emissivity of 0.1, 0.05 and 0.03, respectively.

图1 (a) AM1.5太阳光谱,500 K和600 K时黑体辐射谱,500 K和600 K理想的太阳能选择性吸收曲线分别用蓝色和红色虚线显示.(b) 理想吸收和辐射情况下,不同聚光比下截止波长-温度曲线图.(c) 固定吸收率为0.98,不同辐射率下截止波长-温度曲线图.

0° indicates the incident wave is the transverse magnetic (TM) polarized wave, and that ψ=90° is the transverse electric (TE) polarized wave. Here, the parameters are set as Λ = 400 nm, x = y =150 nm, w = 30 nm, and h = 50 nm, after considering the influence of different parameters.

In 2D periodic structures, the wave vector is specified by the Bloch-Floquent condition[13]:

$$\boldsymbol{K}_{\parallel,mn} = (k_{x,inc} + \frac{2\pi m}{\Lambda_x})\hat{x} + (k_{y,inc} + \frac{2\pi n}{\Lambda_y})\hat{y}, \quad (4)$$

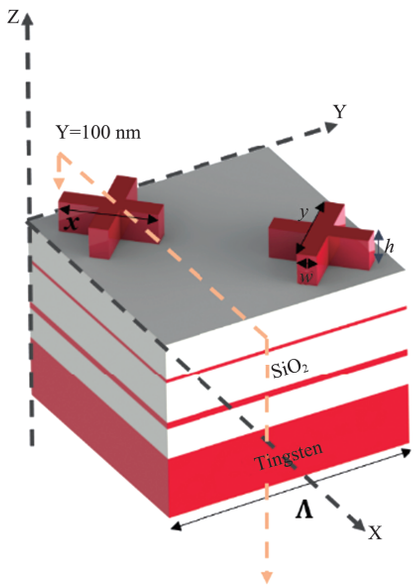

Fig. 2 Schematic design of the 2D periodic twin-crosses tungsten structure being put on the six-layered film structure

图2 基于六层膜的钨基双十字形微结构模型示意图.

where m and n are the diffraction orders in the x and y directions, and Λ_x and Λ_y are the period of the grating along the x and y directions, respectively. $\boldsymbol{K}_{\parallel,mn}$ represents the component of wave vector in the x-y plane. Since $\Lambda_x = \Lambda_y = 400$ nm, when the incident wavelength is greater than 400 nm, $\boldsymbol{K}_{\parallel,mn}$ will be larger than $k_{inc} = 2\pi/\lambda$ for all the diffracted waves except for the zero order (m=0) of diffraction. Thus, all the non-zero diffraction orders would not contribute to the far-field diffuse reflection.

The FDTD method is applied to simulate the absorption properties of the designed metamaterial absorbers in the wavelength region of 0.25~25 μm. The optical constants of tungsten are taken from Palik[14]. The space steps and time steps should satisfy the Courant condition. In addition, in order to obtain the ideal dispersion relation, spatial segmentation should be carried out according to the principle of less than normal grids. The max step should be consistent with the equation $\Delta_{max} = \lambda_{min}/20$ (λ_{min} is the minimum wavelength in the computational region). Thus, in the simulation, the maximum space steps are set as Δx = Δy = 10 nm, Δz = 1 nm, and time step is Δt = 0.003 fs.

2 Results and discussions

By taking the influence of the length, width and thickness of the twin-cross grating into consideration, the parameters of 2D twin-cross grating were set with the values of Λ = 400 nm, $x = y$ =150 nm, w = 30 nm, and h = 50 nm. The performance of this solar selective absorber is presented in Fig. 3. The cut-off wavelength (α = 0.5) is equal to about 1 845 nm, and the weighted average absorptivity is 96.5% in the wavelength region of 250-1 845 nm with the result shown in Fig. 3(a). The weighted absorptivity in average is about 95% in the entire solar radi-

ation region. The calculated emissivity with different temperatures T is shown in Fig. 3(b). The emissivity at 850 K is about 0.086, which is relatively low. By neglecting the conduction heat loss, the total optical-thermal efficiency with the heat radiative loss of SSA could be calculated by

$$\eta_{ot} \approx \alpha - \frac{\varepsilon\sigma_{sb}(T_h^4 - T_{amb}^4)}{C_{opt}q_i} = \alpha\left[1 - \frac{\varepsilon\sigma_{sb}(T_h^4 - T_{amb}^4)}{\alpha C_{opt}q_i}\right], \quad (5)$$

where α and ε present the absorptivity and effective emissivity of the SSA absorber, respectively, σ_{sb} and C_{opt} present the Stefan-Boltzmann constant and optical concentration, respectively, and q_i presents the incident heat flux according to AM1.5 solar spectrum. Taking typical values of q_i = 1 kW/m^2, T_{amb} = 300 K, C_{opt} = 82, the conversion efficiencies are calculated in different temperatures with the results shown in Fig. 3(c). In the assumed conditions, the optical-thermal efficiency of the 2D twin-cross grating in the temperature range of 400~850 K is higher than 86% with w = 30 nm. The optical-thermal efficiency decreases about 5% with temperature increasing from 400 K to 850 K. Due to the symmetrical structure of the 2D twin-cross grating, the spectral absorptivity can be analyzed as the function of wavelength and polarization angle ψ (ψ changes in the range of 0-45°) at normal incidence (θ = 0°) with the result shown in Fig. 3(d). The high absorptivity region represented by red color can be clearly seen and occurs in the 250~1 500 nm wavelength region. The absorptivity spectra are not sensitively affected by changing the polarization angle in the 0~45° range. Thus, the absorber shows the great performance of polarization independence attributed to the four-fold symmetry of the twin-cross grating structure.

In order to further analyze the absorption performance of the PhC-based absorbers with the 2D twin-cross grating structure, the magnetic field is shown at the x-z cross section in the middle of one tungsten cross, namely the cross section Y=100 nm shown in Fig. 2. The contour shows the strength of magnetic field normalized to that of incidence, which is symbolized as $|H_y/H_{inc}|^2$. According to the dispersion relation of surface plasmon polaritons (SPPs), the first order SPPs appear at the wavelength similar to the period[9]. For 2D gratings, SPPs could be excited by both TE and TM waves, and SPPs could propagate along both x and y directions. The dispersion relation of surface plasmons is described as $|\boldsymbol{K}_{spp}| = (\omega/c_o)[\varepsilon_1\varepsilon_2/(\varepsilon_1+\varepsilon_2)]^{1/2}$, where ε_1 and ε_2 represent the permittivity of metal and air, respectively. For TM incident waves, SPPs can be excited when dispersion relation $(\omega/c_o)[\varepsilon_1\varepsilon_2/(\varepsilon_1+\varepsilon_2)]^{1/2}$ equals to $|K_o\sin\theta+2\pi m/\Lambda_x|$ and $[(K_o\sin\theta)^2+(2\pi n/\Lambda_y)^2]^{1/2}$ in x and y direction, respectively. According to Fig. 4(a), obviously there is an absorption peak at about 325 nm. According to the dispersion relation mentioned above, the first SPPs excited near the tungsten-air interface appears at about 394 nm in normal incidence. Most of the energy is concentrated along the tungsten-air interface at the wavelength of

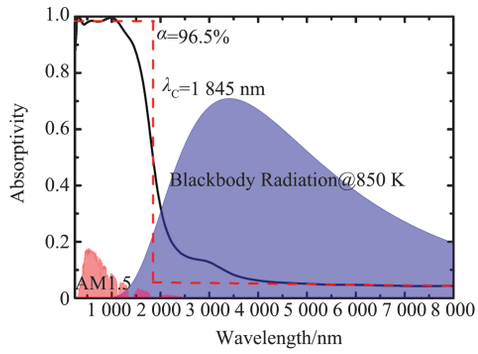

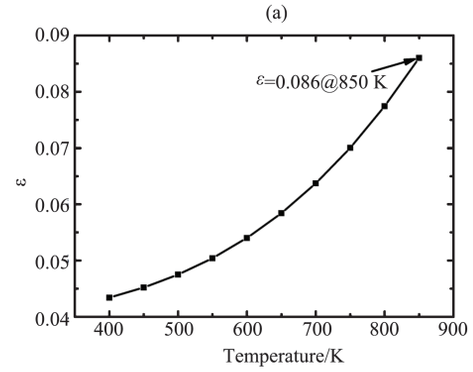

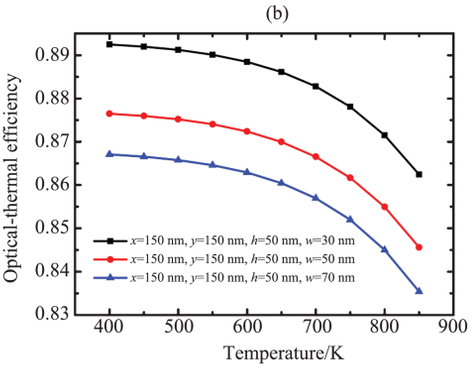

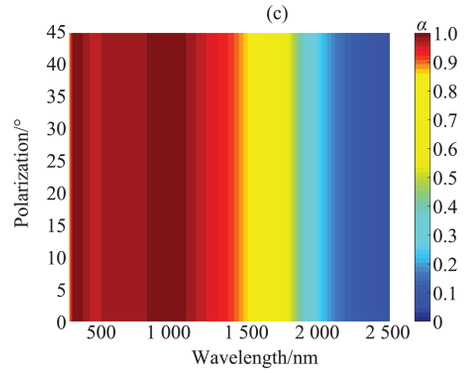

Fig. 3　(a) Absorption spectrum between 250 nm and 8 000 nm with the parameters of the 2D twin-cross grating listed as Λ = 400 nm, x = y =150 nm, w = 30 nm, and h = 50 nm. (b) The calculated emissivity at different temperatures. (c) Optical-thermal efficiency at typically assumed conditions. (d) Contour plot of the absorptivity spectrum as the function of wavelength and polarization angle at the normal incidence condition

图 3　(a) 双十字结构参数为 Λ = 400 nm, x = y =150 nm, w = 30 nm, and h = 50 nm时,250~8 000 nm 波段的吸收曲线图.(b) 计算所得的辐射率-温度曲线.(c)在常规条件下计算所得的光热转换效率-温度曲线.(d)正入射情况下吸收率关于波长和偏振角度的等值线图

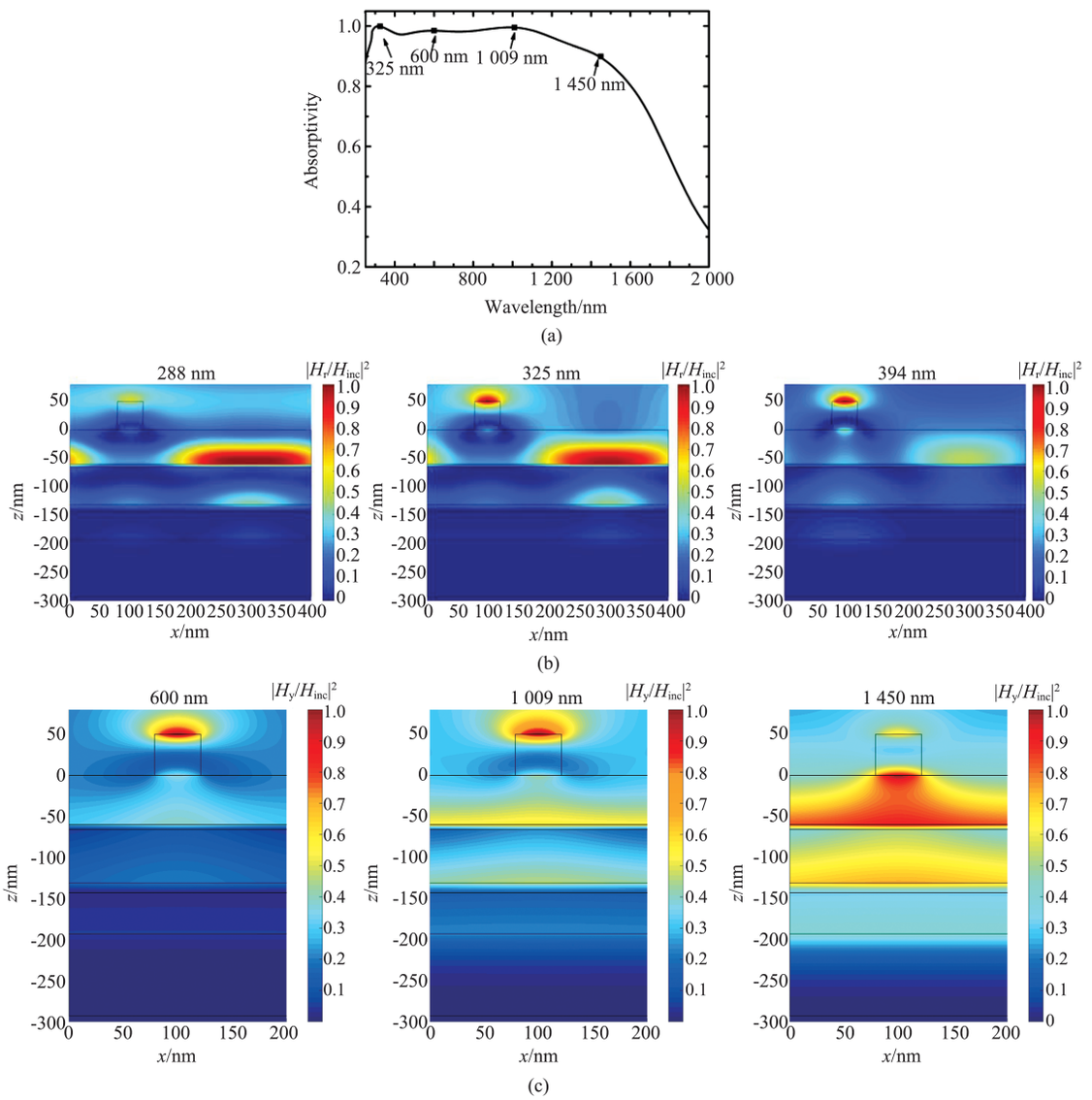

Fig. 4 (a) Absorption spectrum between 250 nm and 2 000 nm in normal incidence condition.(b)Views of the cross-section of electromagnetic field at the wavelength of 288 nm, 325 nm, 394 nm, respectively. (c) Views of the cross-section of electromagnetic field at the wavelength of 600 nm, 1 009 nm, and 1450 nm, respectively

图4 (a)正入射情况下,250~2 000 nm波段的吸收谱图.(b)波长为288 nm,325 nm和394 nm时的电磁场分布纵截面场图.(c)波长为600 nm,1 009 nm和1 450 nm时的电磁场分布纵截面场图

394 nm, as shown in Fig. 4(b). In addition, the calculated SPPs excited at the tungsten-SiO_2 interface seem to occur at the wavelength of about 288 nm in nearly normal incidence condition. Thus, the absorption peak at 325 nm is influenced by SPPs along both of the tungsten-air and tungsten-SiO_2 interfaces, indicating that the energy is largely confined along the tungsten-air and tungsten-SiO_2 interfaces.

Compared to the magnetic field at the wavelength of 320 nm, the magnetic field at 600 nm is partly confined in the SiO_2 layer which is sandwiched between tungsten cross grating and the tungsten layer, as shown in Fig. 4 (c). In addition, the confined energy in the SiO_2 layer is enhanced at 1 009 nm compared to that at 600 nm. The energy is largely confined in the SiO_2 layer at 1 450 nm, which is probably affected by magnetic polariton (MP) resonance. The magnetic polariton resonance is excited by the enhanced magnetic field in the thin dielectric film between two metal films. In fact, the magnetic polaritons are excited because the time-varying magnetic field could induce the electric current at the surface of metals with opposite direction according to Lenz's Law [15-16]. Due to the influence of MP resonance, the absorption of the structure with 2D twin-cross grating is higher than that of just six-layered films around 1 500 nm. It is clear to see that the absorption drops sharply at the wavelengths beyond MP resonance, ensuring the small transition region from high absorption region to low emittance region.

The direction-dependent performance of solar selective absorbers is also a critical issue to affect the solar-thermal application when the solar radiation is incident at oblique angles. The absorption spectra at different inci-

dent angles under both transverse electric (TE) and transverse magnetic (TM) polarizations are further analyzed with the results shown in Fig. 5(a). Under the small incidence angle condition, the absorption spectrum under TM polarization is nearly the same as that under TE polarization. The absorptivity with TE polarization at the incident angle of 50° is a little lower than that with TM polarization. The absorptivities at different incident angles are calculated by averaging the absorptivity under both TM and TE polarization conditions with the results shown in Fig. 5(b). When the incident angle changes from 0 to 30°, the absorption spectra are almost unchanged. At the incident angle of 50°, the high absorptivity in wavelength region of 500~1 000 nm drops by about 3%. Thus, the absorption of designed tungsten-based SSA is insensitive to the incident angle when the incident angle is less than 50°.

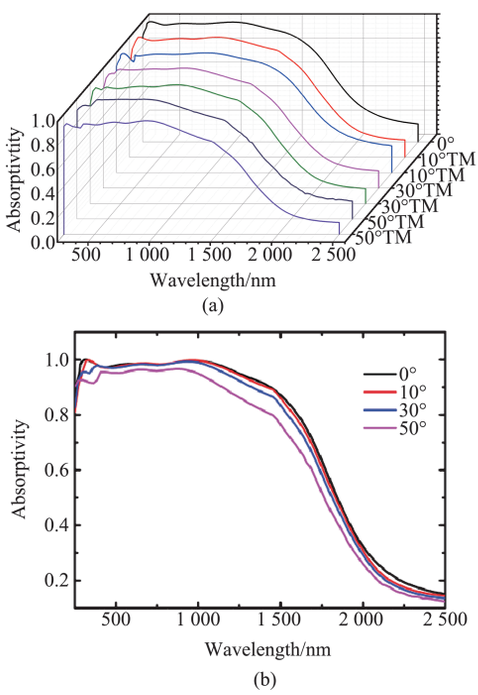

Fig. 5 **(a)** Absorption spectra at different incident angles with TE and TM polarizations. **(b)** Mean absorption spectra at different incident angles
图 5 (a)不同入射角下 TE 和 TM 偏振吸收率-波长曲线.(b)不同入射角下平均吸收率-波长曲线

3 Conclusions

In this work, we designed a PhC-based SSA with the 2D tungsten twin-cross grating structure to fulfill high absorptivity in the solar spectrum region. The calculated cut-off wavelength is around 1.85 μm, suitable for solar-thermal application up to about 850 K. The weighted mean absorptivity before cut-off wavelength is 96.5%, and in the whole solar region is 95%. The calculated emissivity at 850 K is 0.086, working as a reflector in the thermal radiation region. The designed SSA is polarization-independent and great angular-independent up to 50°. Therefore, the PhC-based SSA with the 2D tungsten twin-cross grating structure was proposed potentially suitable for medium-to-high temperature solar application.

References

[1] Weinstein L A, Loomis J, Bhatia B, *et al*. Concentrating Solar Power [J]. *Chemical Reviews*, 2015, **115**(23): 12797-12838.
[2] Hou J Z, Gu D E, Wang T, *et al*. A wide-angle and polarization insensitive highly-tunable infrared metamaterial perfect absorber [J]. *J. Infrared Millim. Waves*, 2015, **34**(4): 406-410.
[3] Kong H, Li G F, Jin Z M, *et al*. Polarization-independent Metamaterial Absorber for Terahertz Frequency [J]. *Journal of Infrared Millimeter and Terahertz Waves*, 2012, **33**(6): 649-656.
[4] Rostamnejadi A, Daneshvar M. Two-dimensional tungsten photonic crystal selective emitter: effects of geometrical parameters and temperature [J]. *Applied Physics B-Lasers and Optics*, 2018, **124**(3): 8.
[5] Nam Y, Yeng Y X, Lenert A, *et al*. Solar thermophotovoltaic energy conversion systems with two-dimensional tantalum photonic crystal absorbers and emitters [J]. *Solar Energy Materials and Solar Cells*, 2014, **122**: 287-296.
[6] Wu D, Liu Y M, Xu Z H, *et al*. Numerical Study of the Wide-angle Polarization-Independent Ultra-Broadband Efficient Selective Solar Absorber in the Entire Solar Spectrum [J]. *Solar Rrl*, 2017, **1**(7): 11.
[7] Stelmakh V, Chan W R, Ghebrebrhan M, *et al*. Sputtered Tantalum Photonic Crystal Coatings for High-Temperature Energy Conversion Applications [J]. *Ieee Transactions on Nanotechnology*, 2016, **15**(2): 303-309.
[8] Sergeant N P, Agrawal M, Peumans P. High performance solar-selective absorbers using coated sub-wavelength gratings [J]. *Optics Express*, 2010, **18**(6): 5525-5540.
[9] Han X, He K B, He Z B, *et al*. Tungsten-based highly selective solar absorber using simple nanodisk array [J]. *Optics Express*, 2017, **25**(24): A1072-A1078.
[10] Wang H, Wang L P. Perfect selective metamaterial solar absorbers [J]. *Optics Express*, 2013, **21**(22): A1078-A1093.
[11] Burlafinger K, Vetter A, Brabec C J. Maximizing concentrated solar power (CSP) plant overall efficiencies by using spectral selective absorbers at optimal operation temperatures [J]. *Solar Energy*, 2015, **120**: 428-438.
[12] Cao F, McEnaney K, Chen G, *et al*. A review of cermet-based spectrally selective solar absorbers [J]. *Energy & Environmental Science*, 2014, **7**(5): 1615-1627.
[13] Zhao B, Wang L P, Shuai Y, *et al*. Thermophotovoltaic emitters based on a two-dimensional grating/thin-film nanostructure [J]. *International Journal of Heat and Mass Transfer*, 2013, **67**: 637-645.
[14] D P E. Handbook of optical constants of solids II [J]. *Boston Academic Press*, 1991, **1**(1):77-135.
[15] Khodasevych I E, Wang L P, Mitchell A, *et al*. Micro- and Nanostructured Surfaces for Selective Solar Absorption [J]. *Advanced Optical Materials*, 2015, **3**(7): 852-881.
[16] Lee B J, Wang L P, Zhang Z M. Coherent thermal emission by excitation of magnetic polaritons between periodic strips and a metallic film [J]. *Optics Express*, 2008, **16**(15): 11328-11336.